JOURNAL OF GUIDANCE, CONTROL, AND DYNAMICS
Vol. 26, No. 6, November–December 2003

Improved Clearance of a Flight Control Law Using μ-Analysis Techniques

Declan G. Bates* and Ridwan Kureemun†
University of Leichester, Leichester, England LE1 7RH, United Kingdom
and
Thomas Mannchen‡
University of Stuttgart, 70550 Stuttgart, Germany

Some new tools are described for the clearance of flight control laws for highly augmented aircraft. The tools are developed from general μ-analysis methods and are applied to the clearance of a flight control law for a vertical/short takeoff and landing aircraft. Criteria and methods currently used in the industrial flight control law clearance process are described in detail. A physical approach to linear fractional transformation based uncertainty modeling is applied and validated on the nonlinear aircraft model. Stability robustness analysis results for the flight control law are presented in terms of the standard clearance criteria currently used by the European aerospace industry. Comparisons of the results obtained using μ-analysis and current approaches reveal that the new μ tools provide more rigorous and efficient analysis of worst-case aircraft stability characteristics in the presence of multiple sources of parametric uncertainty.

I. Introduction

MODERN high-performance aircraft are often designed to be naturally unstable due to performance reasons and, therefore, can only be flown by means of a controller that provides artificial stability. Because the safety of the aircraft is dependent on the controller, it must be proven to the clearance authorities that the controller functions correctly throughout the specified flight envelope in all normal and various failure conditions and in the presence of all possible parameter variations.

This task is a very lengthy and expensive process, particularly for high-performance aircraft, where many different combinations of flight parameters (e.g., large variations in mass, inertia, center of gravity positions, highly nonlinear aerodynamics, aerodynamic tolerances, air data system tolerances, structural modes, failure cases, etc.) must be investigated so that guarantees about worst-case stability and performance can be made.

The aircraft models used for clearance purposes describe the actual aircraft dynamics, but only within given uncertainty bounds. One reason for this is the limited accuracy of the aerodynamic data set determined from theoretical calculations and wind-tunnel tests. These parameters can even differ between two aircraft of the same type, due to production tolerances. Moreover, the employed sensor, actuator, and hydraulic models are usually only approximations, where the nonlinear effects are not fully modeled because they are either not known or it would make the model unacceptably complex.

The goal of the clearance process is to demonstrate that a set of selected criteria expressing stability and handling requirements is fulfilled. Typically, criteria covering both linear and nonlinear stability, as well as various handling and performance requirements, are used for the purpose of clearance. The clearance criteria can be grouped into four classes: 1) linear stability criteria, 2) aircraft handling/pilot induced oscillation criteria, 3) nonlinear stability criteria, and 4) nonlinear handling criteria. This paper focuses on the use of new analysis techniques for two linear stability criteria, which are described in detail in the next section. Details of the other clearance criteria may be found in Ref. 1.

To perform the clearance, for each point of the flight envelope, for all possible configurations, and for all combinations of parameter variations and uncertainties, violations of the clearance criteria and the worst-case result for each criterion must be found. Based on the clearance results, flight restrictions are imposed where necessary. Faced with limited time and resources, the current flight clearance process employed by the European aerospace industry uses a gridding approach,[1] whereby the various clearance criteria are evaluated for all combinations of the extreme points of the aircraft's uncertain parameters. This process is then repeated over a gridding of the aircraft's flight envelope. Clearly, the effort involved in the resulting clearance assessment increases exponentially with the number of uncertain parameters. Another difficulty is that there is no guarantee that the worst-case uncertainty combination has in fact been found because 1) it is possible that the worst-case combination of uncertain parameters does not lie on their extreme points and 2) only a few selected points in the aircraft's flight envelope can be checked. In this paper, a new approach to the clearance problem is described, based on the use of the structured singular value analysis method. The proposed approach is shown to have the capability to improve both the reliability and efficiency of the current flight clearance process.

The paper is organized as follows. In Sec. II the clearance criteria addressed in this study are described. Section III gives details of the vectored-thrust aircraft advanced flight control (VAAC) Harrier aircraft model and control law. In Sec. IV, the problem of generating accurate linear fractional transformation- (LFT-) based uncertainty models for the VAAC Harrier aircraft is discussed. In Sec. V, the μ-analysis tools used to address the clearance criteria considered in this study are described. In Sec. VI, clearance results are presented using both the classical and μ-analysis approaches. Finally, in Sec. VII, some conclusions are presented.

II. Linear Stability Clearance Criteria

In this section, we give a brief description of the two linear stability criteria addressed in this paper. Further details of these and other clearance criteria may be found in Ref. 1.

Received 9 December 2002; revision received 30 May 2003; accepted for publication 25 June 2003.

*Lecturer, Department of Engineering; dgb3@le.ac.uk.
†Research Associate, Department of Engineering.
‡Research Engineer, Institute of Flight Mechanics and Control, Pfaffenwaldring 7a.

A. Stability Margin Criterion

A basic requirement of the flight clearance process is to prove that the aircraft is stable over the entire flight envelope with sufficient margin against instability for all known uncertainties (worst-case combinations). The process consists of calculating linear stability margins for the open-loop frequency response in pitch, roll, and yaw. These frequency responses are obtained by breaking the loop at the input of each actuator or of each sensor and then are plotted in Nichols diagrams, where the required phase and gain margins are shown as exclusion regions, which must not be violated by the plot.

In single-loop analysis, the open-loop frequency response is obtained by breaking the loop at the input of each actuator or sensor, one at a time, while leaving the other loops closed. For the nominal case, these Nichols plots should not violate the outer exclusion region shown in Fig. 1, which corresponds to a minimum gain margin of ± 6 dB and a minimum phase margin of ± 35 deg. When uncertainties are taken into account, a boundary corresponding to ± 4.5 dB is used, as shown by the inner exclusion region in Fig. 1.

In multiloop analysis, the closed-loop system is required to withstand the application of simultaneous gain and phase offsets, defined by the regions shown in Fig. 2, at the actuators or sensors without becoming unstable. To test for violations of this criterion, a perturbation of the form $K[(1 - Ts)/(1 + Ts)]$ is inserted at, for example, the input of each actuator. With K set to 1, T is then varied

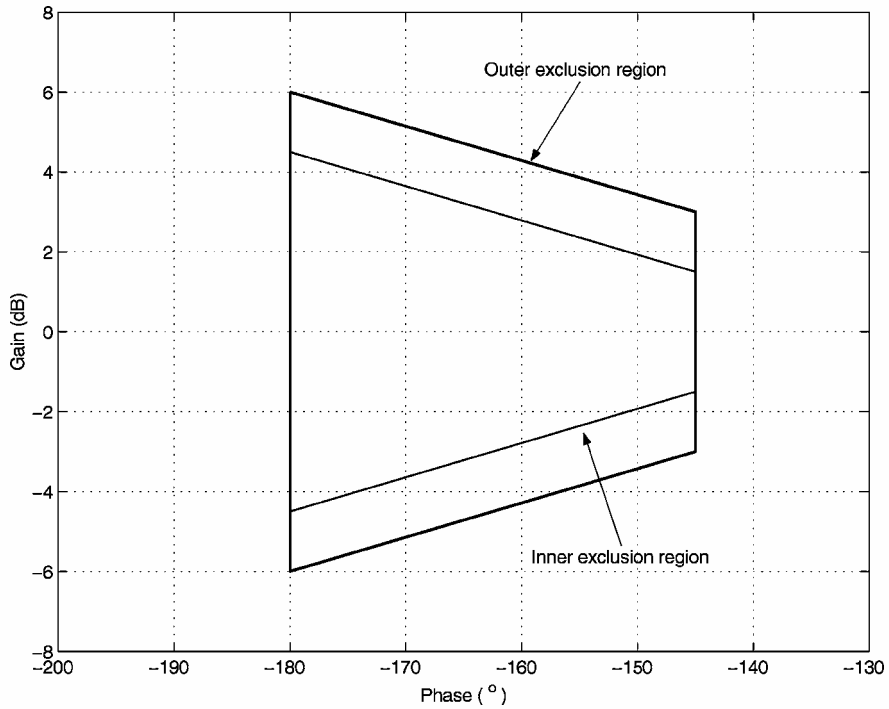

Fig. 1 Nichols stability margin boundaries (single-loop analysis).

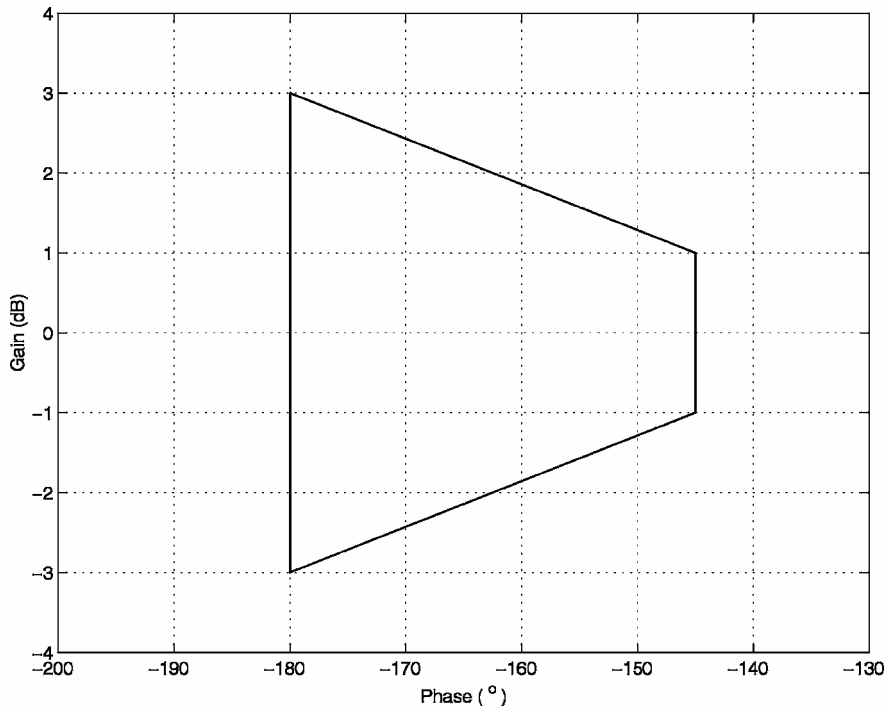

Fig. 2 Nichols stability margin boundaries (multiloop analysis).

simultaneously in each loop until the eigenvalues of the closed-loop system go unstable. The phase margin is calculated as

$$\phi_{\mathrm{PM}} = 2 \times \tan^{-1} \omega T \tag{1}$$

where ω is the frequency of the generated undamped oscillation. K is then increased and decreased by 1 dB (corresponding to the right corner points of the Nichols exclusion region shown in Fig. 2) and T is again varied for the new fixed gain until the eigenvalues become unstable. When $T = 0$ and K is varied, the upper and lower gain margins can be obtained (corresponding to the left corner points of the Nichols diagram). These steps can be repeated for any number of points around the required Nichols exclusion region. Because the criterion must be evaluated over all combinations of the aircraft's uncertain parameters, this test is in practice usually restricted to only a few points of the exclusion regions, for example, the four corners of each exclusion region. In addition, the same gain and phase offsets are usually applied simultaneously in all loops, to avoid testing over too large a number of different combinations. Hence, it can be argued that this method can in practice lead to optimistic results.

B. Worst-Case Eigenvalue Criterion

In addition to the stability margin criterion, the eigenvalues of the closed-loop system must be calculated to identify possible unstable, that is those with positive real part, eigenvalues that do not appear in the Nichols plots. It is required to identify the flight cases where unstable eigenvalues occur and for what tolerance combination these eigenvalues have the largest real part. This test aims to determine the most severe cases of divergent modes in the closed-loop system to allow an assessment of their acceptability in terms of their influence on aircraft handling. A typical boundary on the real part of the eigenvalues is shown in Fig. 3.

Note that, for real eigenvalues, the definition of worst case as the maximum real part among the positive eigenvalues is straightforward. For complex eigenvalues, different definitions of worst cases can be chosen, such as the magnitude of the complex eigenvalue. Usually, the maximum positive real part is selected because it can be directly linked to existing handling qualities requirements on the minimum time to double amplitude of unstable modes.

III. VAAC Harrier Wide-Envelope Model Aircraft and Control Law

The Harrier wide-envelope model (HWEM) is a full nonlinear model of the VAAC Harrier, developed by QinetiQ, Ltd., for research on various aspects of flight control that are relevant to short takeoff and vertical landing operations. Recent research milestones with the VAAC Harrier include the first reported flight of an H^{∞} control law,[2] and the first reported flight of a linear parameter varying control law.[3] For the purposes of this study, the HWEM, originally implemented as a FORTRAN program, has been converted to a pure SIMULINK model. Data for the model was derived from a variety of sources, such as wind-tunnel and flight-test measurements and theoretical predictions, obtained from various aircraft.[4] The flight control surfaces comprise an all-moving tailplane, ailerons, flaps, rudder, and airbrake. With the exception of the rudder, all control surfaces are hydraulically powered. The powerplant is a Rolls–Royce Pegasus Mk. 103 turbofan with four separate but coupled nozzles that allow the direction of the thrust to be altered. High-pressure bleed air from the engine compressor provides control at low speeds and hover, when the aerodynamic control surfaces become ineffective. The bleed air is ejected through reaction control valves (RCVs) in the wing tips (roll control), nose (pitch control), and tail boom (pitch and yaw control). Because the RCVs are mechanically linked to the appropriate control surfaces, the need for additional controls/actuators is avoided. Bleed air to the RCVs becomes progressively available as the nozzle angle is increased, the system being fully pressurized when nozzle angle exceeds 34 deg.

When engaged, the flight control system (FCS) has full authority over all surfaces, except the airbrake, and engine control extends to the throttle and nozzles. In addition, the FCS can also control the roll and yaw autostab servos, which provide limited authority control of the ailerons and yaw RCVs, respectively.

The aircraft's dynamic behavior can be categorized by three modes: a conventional takeoff and landing mode in which the nozzles are at 0 deg relative to the horizontal body axis, a vertical take-off and landing mode in which the nozzles are at an angle of 90 deg, and finally a transition mode in which the nozzles are between 0 and 90 deg.

The flight control law for the HWEM analyzed in this study is based on VAAC CL002. It is a full three-axis (pitch, roll, and yaw) control law designed using classical methods. The study reported in this paper considers the pitch axis only. (For more details of

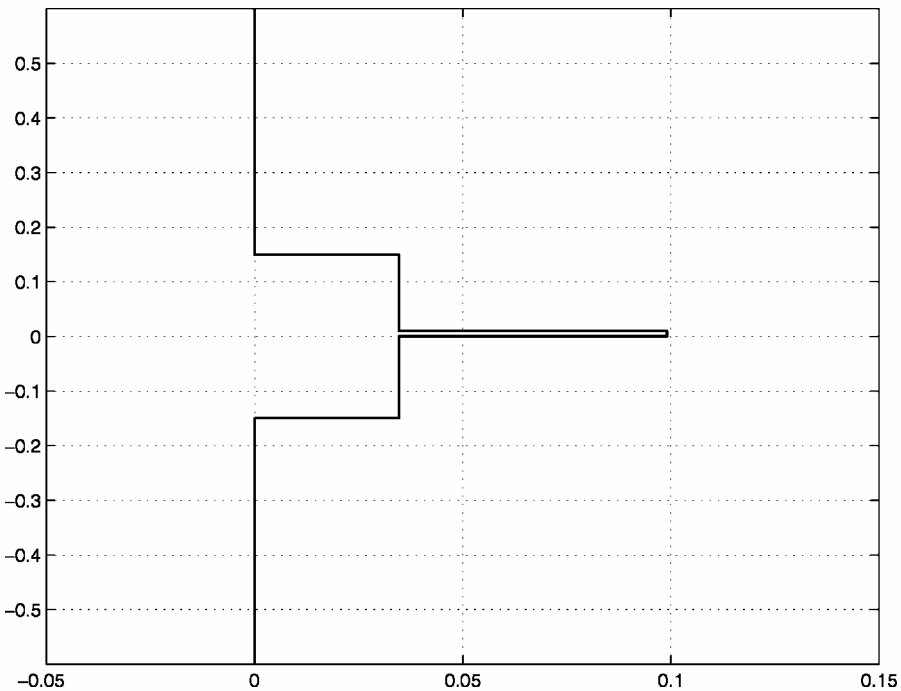

Fig. 3 Boundaries for the unstable eigenvalue requirement.

Table 1 Flight envelope for the HWEM

FC	Airspeed, kn
FC1	200
FC2	150
FC3	130
FC4	110
FC5	90
FC6	60
FC7	0.01

Table 2 Most relevant longitudinal uncertainties

Parameter	Variable name	[Min, max] value
Longitudinal position of center of gravity, % mean aerodynamic chord	U_X_{cg}	$[-1.72, -11.7]$
Pitch moment of inertia, kg m^2	U_I_{yy}	[56887, 69529]
Uncertainty on tailplane effectiveness, %	$U\_C_{m_{tail}}$	$[-20, +20]$
Uncertainty on pitching moment due to pitch rate, %	$U\_C_{m_q}$	$[-20, +20]$
Uncertainty on pitching moment due to α, %	$U\_C_{m_\alpha}$	$[-20, +20]$

the lateral/directional control laws refer to Ref. 4. CL002 emulates the standard Harrier's three-inceptor pitch control strategy but with some additional augmentation to reduce pilot workload. The longitudinal stick commands pitch rate with pitch attitude hold above 60 knots indicated airspeed (KIAS), blending to pitch attitude command below 50 KIAS. The pitch attitude hold function engages when the stick is centered, provided the undercarriage is down and airspeed is below 250 KIAS. In the hover, the datum attitude, corresponding to stick-free attitude, is preset to 7.5 deg (approximately the normal landing attitude of the Harrier). Thrust magnitude and direction are controlled conventionally, using the throttle and nozzle levers, respectively. Additional pitch law features include the decoupling of pitch from thrust vector and flap angle changes, automatic flap scheduling, and bank compensation to supply the pitch rate required to maintain level flight in a banked turn.

Points in the flight envelope of the HWEM to be analyzed in the clearance task are given in Table 1. All flight conditions are defined for 1-g straight and level flight at an altitude of 200-ft above mean sea level. The angle-of-attack range for all flight conditions is $[-4, +16]$ deg. Five category 1 (most significant) uncertain parameters are specified for the longitudinal axis analysis and are shown in Table 2. Further information about the uncertain aircraft parameters may be found in Refs. 4 and 5.

IV. LFT-Based Uncertainty Modeling

To apply μ-analysis tools to the HWEM model, the uncertainties in the original nonlinear aircraft model must be represented in the form of LFTs. In fact, it can be argued that the major difficulty in applying μ-analysis methods to real-world applications lies in this initial modeling step. In recent years, the subject of LFT-based uncertainty modeling has received much attention and has been found to be a very deep problem. (See Ref. 6 for an overview.) For aerospace systems, obtaining a unique linear model based on an LFT description of the uncertainties, which covers a range of flight conditions and possible parameter variations, is an extremely challenging modeling task. Different techniques for generating LFT-based uncertainty models have their advantages and disadvantages, and their application is geared toward the nature of the problem being considered. For instance, in the flight clearance process, the usefulness of the chosen modeling technique is assessed on characteristics such as the conservatism of the method, the ability to identify the worst-case parameter combination, the computation time and effort required, and finally the complexity involved in the implementation.

LFT-based uncertainty models can be derived for both linear and nonlinear systems. For linear systems, LFT-based uncertainty models can be derived numerically or physically from a given set of linearized equations of motions. The method necessitates the uncertain aircraft parameters to be explicitly defined in the equations of motion and is generally easy to implement. For nonlinear systems, the problem of generating accurate LFT-based uncertainty models is much more difficult. In general, three different approaches can be identified: 1) numerical methods,[7–9] 2) symbolic linearization methods,[7,10] and 3) physical modeling methods.[6,11]

Numerical approaches are useful when precise information about the way in which the uncertain aircraft parameters enter the aircraft dynamic equations is not known. This may be due to lack of knowledge about the precise effect of these parameters and/or difficulties with the software used to construct the aircraft model and its various subsystems. These techniques use the differences in the linearized trims that arise from the nonlinear simulation model of the aircraft evaluated over all combinations of the extreme points of the uncertain parameters. These models form a so-called multimodel state description,

$$\delta\dot{x}(t) = A_i\delta x(t) + B_i\delta u(t), \qquad \delta y(t) = C_i\delta x(t) + D_i\delta u(t) \quad (2)$$

For each varying element of each state-space matrix, it is then possible to calculate its minimum, for example, $a_{ij}^{\min}$; maximum, for example $a_{ij}^{\max}$; and nominal, for example, $(a_{ij}^{\max} + a_{ij}^{\min})/2$ values. The multimodel system (2) can, thus, be replaced by an affine parameter-dependent representation of the form

$$\begin{bmatrix} A & B \\ C & D \end{bmatrix} = \begin{bmatrix} A_0 & B_0 \\ C_0 & D_0 \end{bmatrix} + \sum_{i=1}^{n_A} \Delta_i \begin{bmatrix} A_i & 0 \\ 0 & 0 \end{bmatrix} + \sum_{i=n_A+1}^{n_B} \Delta_i \begin{bmatrix} 0 & B_i \\ 0 & 0 \end{bmatrix}$$

$$+ \sum_{i=n_B+1}^{n_C} \Delta_i \begin{bmatrix} 0 & 0 \\ C_i & 0 \end{bmatrix} + \sum_{i=n_C+1}^{nD} \Delta_i \begin{bmatrix} 0 & 0 \\ 0 & D_i \end{bmatrix} \quad (3)$$

(A_0, B_0, C_0, D_0), thus, corresponds to the new nominal system. Then, for each varying entry in the matrix A, for example, we have a Δ_i and an A_i in expression (3), where Δ_i is an uncertain real scalar parameter that varies between 1 and -1 and A_i is equal to $[(a_{ij}^{\max} - a_{ij}^{\min})/2]$. For a model in this form, the well-known Morton's method[12] then allows an LFT-based uncertainty model to be easily generated.

The approach just described is fast and easy to implement. Also, quantities such as Mach number and altitude can be easily incorporated in the vector of unknown parameters to generate LFT-based uncertainty models that are valid over particular regions of the flight envelope. Given a good trimming routine, this entire process can be fully automated. Moreover, a knowledge of the explicit relationship between each uncertain model parameter and each element of the system state-space matrices is not required, thus greatly simplifying the task of LFT-based uncertainty modeling. The resulting parametric model covers all possible linearizations arising from the uncertain nonlinear model. However, this representation of physical uncertainties may be conservative because possible joint parameter dependencies among the state-space elements in the model will be ignored. It also means that, although we can identify the worst-case state-space system for a given criterion, we cannot trace this back to identify the corresponding worst-case uncertainty in terms of the actual uncertain aircraft parameters. A partial solution to the described problems is provided by the approach in Ref. 9, which seeks to find trends established by the dependency of the state-space elements on the uncertain parameters by making use of compensation parameters. Each compensation parameter acts independently on one state-space matrix element. In general, these trends are modeled by a multidimensional regression plane, which describes the linear variation, and a band structure that is limited by planes parallel to the regression plane, above and below, to include nonlinear deviations. The actual value of the uncertain state-space element is then assumed to lie somewhere within this band structure. When this approach is used, the sizes of the uncertainty bands are reduced, thus, decreasing conservatism. Moreover, the trends and bands method allows the computation of the worst case in terms of the actual physical uncertain parameters.

A second possible approach to LFT-based uncertainty modeling for nonlinear systems is based on symbolic linearization methods. The approach requires the construction of the nonlinear aircraft model solely in terms of nonlinear dynamic equations, which explicitely contain the uncertain aircraft parameters in a rational form. Once these equations have been validated against the original nonlinear model, they can be entered as symbolic objects in MAPLE or MATLAB® (using the Symbolic Math Toolbox). Symbolic linearization is then performed to obtain a linearized LFT-based uncertainty model.

The advantage of this method is that the resulting uncertainty model allows the computation of the exact worst-case set of uncertainties in terms of the actual uncertain flight parameters. However, the modeling effort involved can be substantial, and because of their complexity, many of the nonlinear equations may have to be further simplified before the symbolic linearization is performed. For example, many stability derivatives (such as the pitching moment coefficients, yawing moment coefficients, etc.) can be complex functions of the flight parameters, and it is common practice to model them by means of look-up tables. In many cases, finding a relationship between these elements can be nontrivial and may involve deep investigation. Even if interpolation is used to find a polynomial fit to the data, it is necessary to focus on only a certain range of variation of the flight parameters to keep the complexity of the resulting equations, that is, the order of the polynomials, to a minimum. Thus, an error margin will exist between these interpolations and the actual behavior of the original parameters. Inevitably, inappropriate assumptions may well lead to a significant loss of accuracy, which is then reflected in the final LFT-based uncertainty model, leading to analysis results that are overly optimistic or conservative. Although compensation parameters can be used to reduce the error margins, this tuning process can be very time consuming. Furthermore, the interpolation process is often trim dependent, that is, the trim values of some flight parameters may be necessary to generate the polynomial fits. Obviously, the resulting analytical model will then only be valid in a close neighborhood of the trimpoint where it has been derived. Incidently, this also means that changing the trimpoint may bring drastic changes to the behavior of the model so that the whole interpolation procedure has to be repeated again. Further discussion of the application of this modeling approach to the HWEM aircraft model may be found in Ref. 13.

A third approach to generating LFT-based uncertainty models, and the one applied in this paper, is that based on physical modeling principles. In this approach, the uncertainties are directly introduced in the nonlinear SIMULINK model of the aircraft in the form of multiplicative (or additive) uncertainties. Consider, for example, that the pitch moment coefficient due to tailplane deflection, $C_{M_{\text{tail}}}$, is subject to uncertainty of $\pm 20\%$. We can, therefore, write $C_{M_{\text{tail}}} = C^0_{M_{\text{tail}}}(1 + U\_C_{M_{\text{tail}}}\Delta_1)$, where $C^0_{M_{\text{tail}}}$ is the nominal value of $C_{M_{\text{tail}}}$, $U\_C_{M_{\text{tail}}}$ is a weight on the uncertainty, where $U\_C_{M_{\text{tail}}} = 0.2$ in this case, and Δ_1 varies in the interval $[-1, 1]$. Note that any variation in a parameter of the form $x_{\min} \le x \le x_{\max}$ can be written as just given in terms of a nominal value and a weighted uncertainty in the interval $[-1, 1]$. Now, the uncertainty in the aircraft dynamics due to $C_{M_{\text{tail}}}$ can be represented physically in block diagram form as shown in Fig. 4. In Fig. 4, we have added an extra fictitious input and output, w_1 and z_1, respectively, at the point in the system where the uncertainty Δ_1 occurs. This step is then repeated for each Δ_i representing the uncertainty in the other uncertain parameters. Now using standard block diagram manipulation software, for example, the function linmod in MATLAB, the resulting nonlinear model can be linearized to calculate the transfer matrix of the system M with inputs $u = [w_1, \ldots, w_n, u_c]$ and outputs $y = [z_1, \ldots, z_n, y_m]$, where u_c are the control inputs and y_m are the measured outputs. The LFT-based uncertainty model for the system, shown in Fig. 5, is then given by the relation

$$y_m = F_u[M(s), \Delta]u_c \tag{4}$$

where $\Delta = \text{diag}(\Delta_1, \ldots, \Delta_n)$

Clearly, the outlined approach is simple and intuitive and allows an exact description of joint parametric dependencies in the model. Thus, it can be used to nonconservatively model the effect of the parametric uncertainties on the closed-loop system. As a result, the exact worst-case set of uncertain parameters can be computed. If each uncertainty is introduced in only one location in the SIMULINK block diagram, the resulting LFT-based uncertainty model will also be of minimal order. In addition, this physical

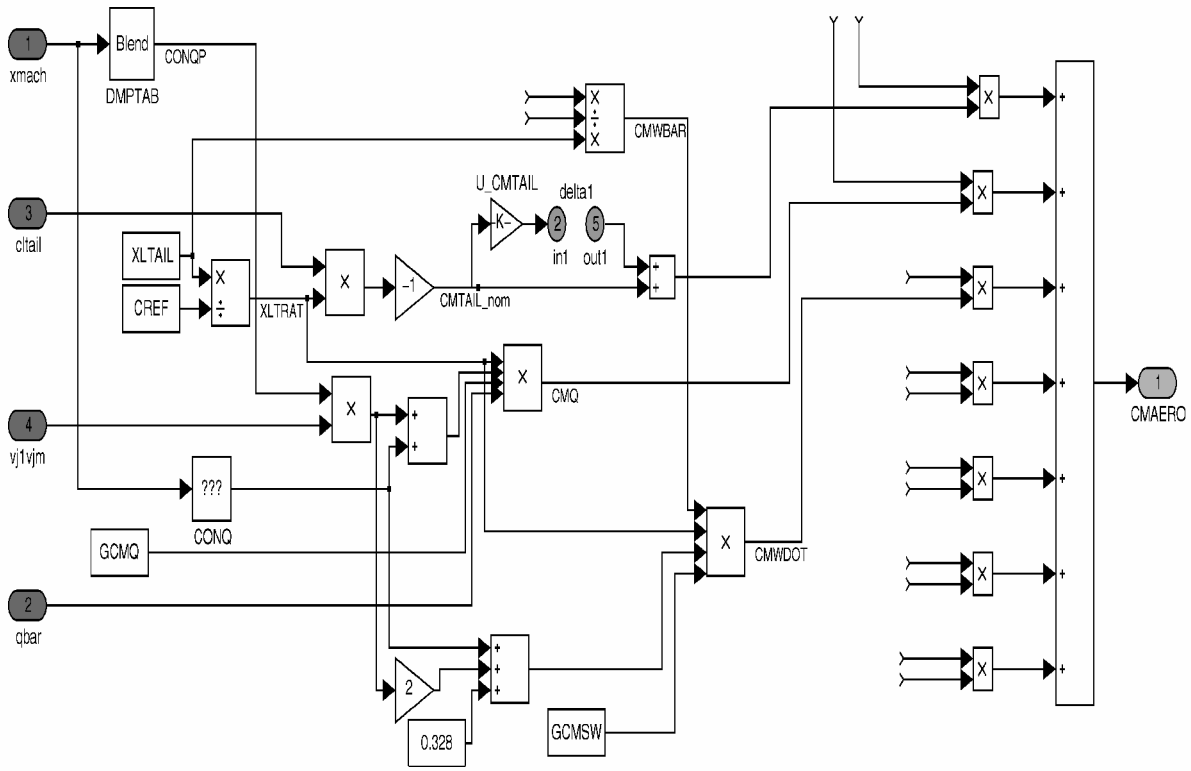

Fig. 4 Part of the HWEM model with uncertainty included.

modeling approach allows additional uncertainties in the physical parameters (such as products of the uncertainties) to be easily implemented in the model.

The main limitation of the approach is that detailed information about the model and the uncertainties is required. Hence, its application is restricted to those models that can be implemented in a SIMULINK block diagram representation. Another drawback is that the dependence of the linearizations on the uncertain parameters is ignored, and therefore, it is not clear how an LFT-based uncertainty model could be generated to capture variations in flight parameters such as the angle of attack or Mach number. Thus, unlike with numerical modeling approaches, it is not possible to easily generate LFT-based uncertainty descriptions that are valid over particular regions of the flight envelope.

To determine the accuracy of the derived LFT-based uncertainty model, it is vital, before any analysis, to validate it against the original linearized and nonlinear model. Time-domain simulations are particularly suited for this purpose, although further analysis such as eigenvalue comparisons can also be carried out. Initially, the nominal case (where all of the uncertainties are set at their nominal values) is considered, but this can be easily extended to take into account any combination of the uncertainties within their ranges. We illustrate the process for an LFT-based uncertainty model of the HWEM generated at FC2. The five category 1 longitudinal uncertainties from Table 2 are considered, and responses for inputs on tailplane, nozzle angle, and throttle were generated.[13] Sample results for a 1-deg step input to the tailplane are shown in Fig. 6. Figure 7 shows the same case when a random combination of the uncertainties was used. In general, for small inputs, a good match was obtained between the nonlinear and LFT-based models, although the match is not as good for random values of the uncertainties (Fig. 7) as it is for the nominal case (Fig. 6). This is to be expected, because the LFT-based model always uses the same linearization, which would, of course, be changed by the variations in the uncertain parameters of the nonlinear model. A final check of the LFT-based model can be performed by comparing the closed-loop characteristics of the models. Figure 8 shows the closed-loop pitch rate responses to a step demand on pitch rate, which again shows good matches between the various models.

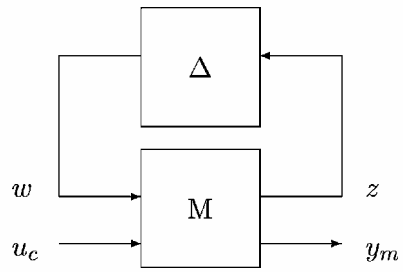

Fig. 5 Upper LFT uncertainty description.

V. Evaluating Clearance Criteria with μ-Tools

In this section, we describe how general μ-analysis methods can be adapted to address the particular clearance criteria defined in Sec. II. For the worst-case stability margin criterion, we shall show that μ has a straightforward interpretation in terms of classical gain/phase margin and Nichols exclusion region robustness specifications. In addition, evaluation of μ away from the $j\omega$ axis provides an efficient test for the worst-case eigenvalue criterion. In fact, μ analysis provides the capability to test efficiently for violations of both criteria, for all possible combinations of parametric uncertainty, without resorting to the gridding approach traditionally used by industry.

A. Elliptical Nichols Plane Exclusion Regions μ Analysis

In this approach, first proposed in Refs. 14 and 15, the original Nichols exclusion regions shown in Fig. 1 are replaced with elliptical

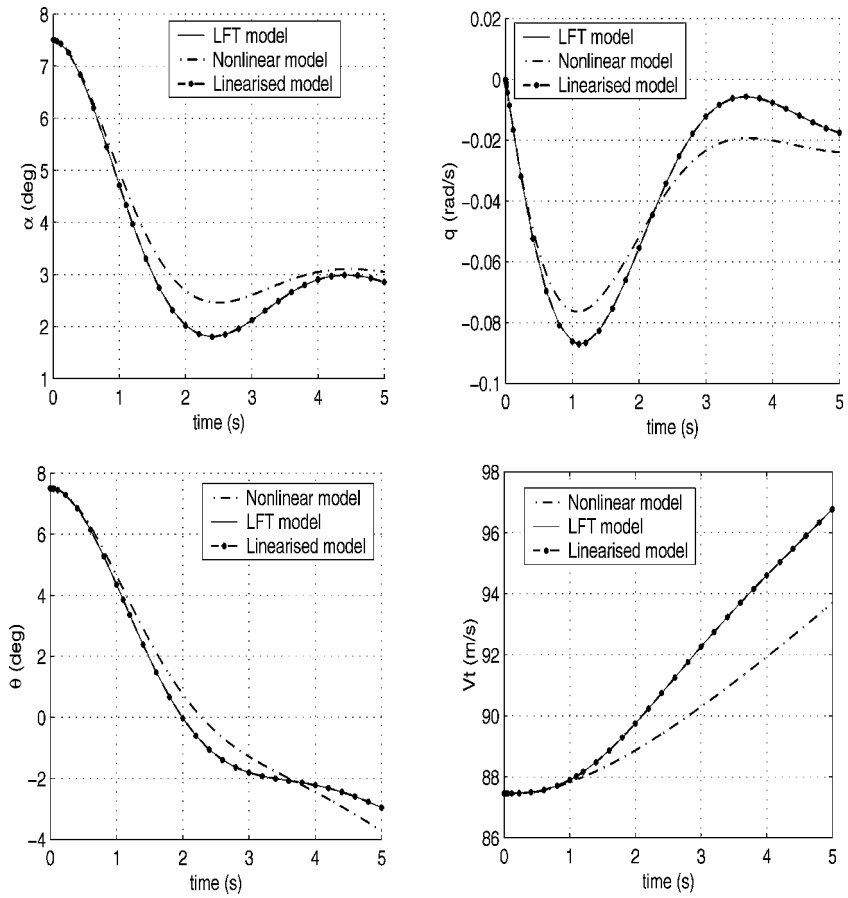

Fig. 6 Responses to a 1-deg step demand on tailplane (nominal case).

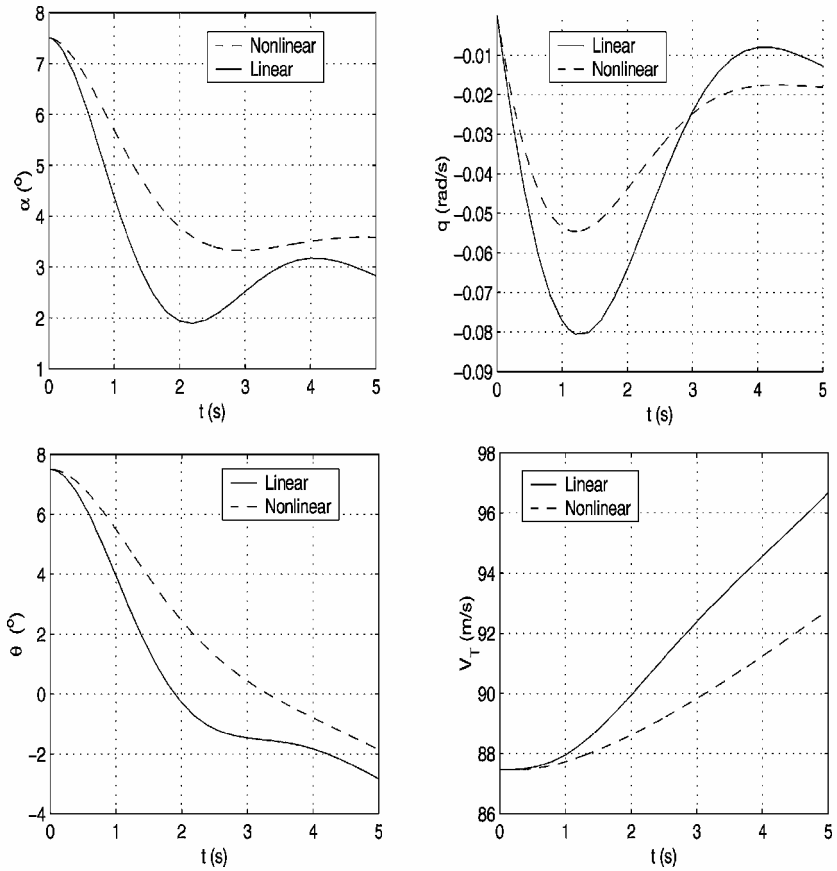

Fig. 7 Responses to a 1-deg step demand on tailplane for random values of the uncertainties.

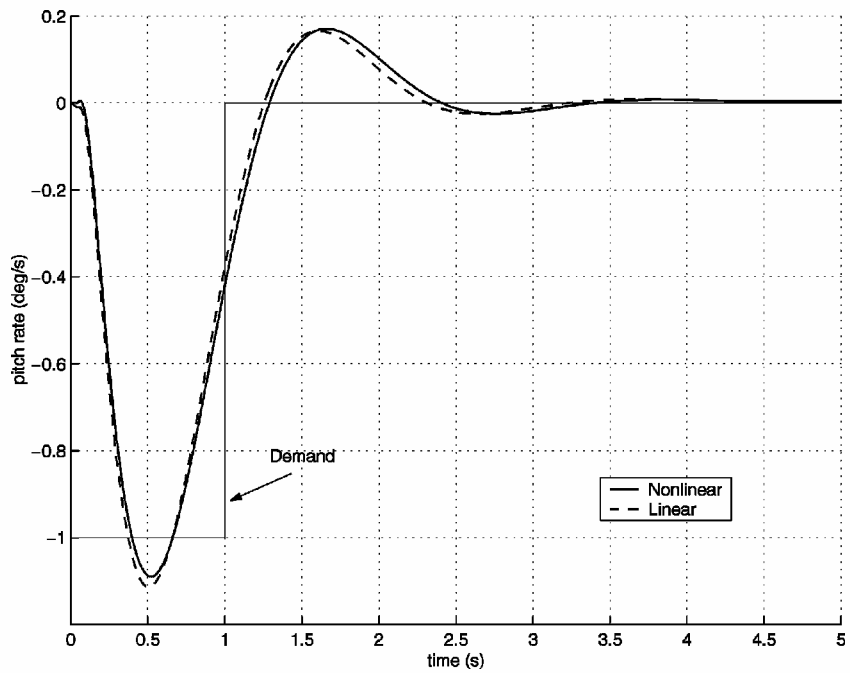

Fig. 8 Pitch rate responses to a step demand on pitch rate.

regions of the form shown in Fig. 9. These elliptical regions are centered around the critical point $(-180, 0)$ and satisfy the equation

$$|L(j\omega)|^2_{\text{dB}} \big/ G_m^2 + (\angle L(j\omega) + 180)^2 \big/ P_m^2 = 1 \qquad (5)$$

where $L(j\omega)$ is the open-loop frequency response, G_m is the desired gain margin, and P_m is the desired phase margin.

Thus, for example, any feedback system whose open-loop frequency response avoids the regions A and B in Fig. 9 provides gain and phase margins of ± 6 dB/± 36.87 deg and ± 4.5 dB/± 28.44 deg, respectively. (Note that these values are very close to those required under the classical exclusion regions defined in Sec. II). Note that for these particular choices of gain and phase margins the corresponding exclusion regions in the Nyquist plane are circles with (center, radius) given by $(-1.25, 0.75)$ for region A, and $(-1.14, 0.54)$ for region B (Refs. 14 and 13) (Fig. 10).

Now, as shown in Ref. 14, another way to interpret the requirement for avoidance of, for example, the circle B in the Nyquist plane

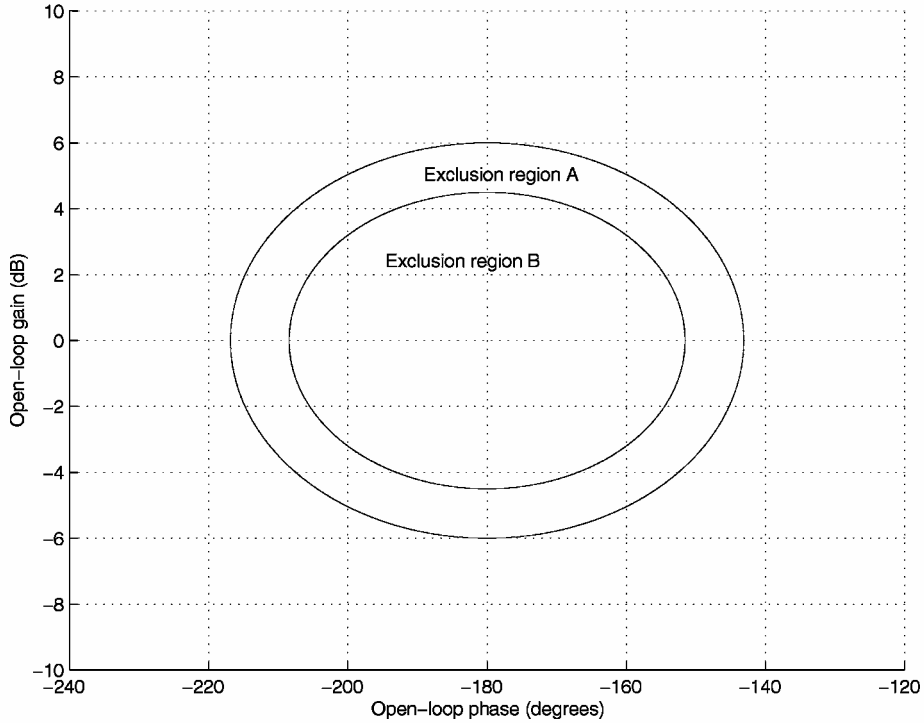

Fig. 9 Elliptical Nichols plane exclusion regions.

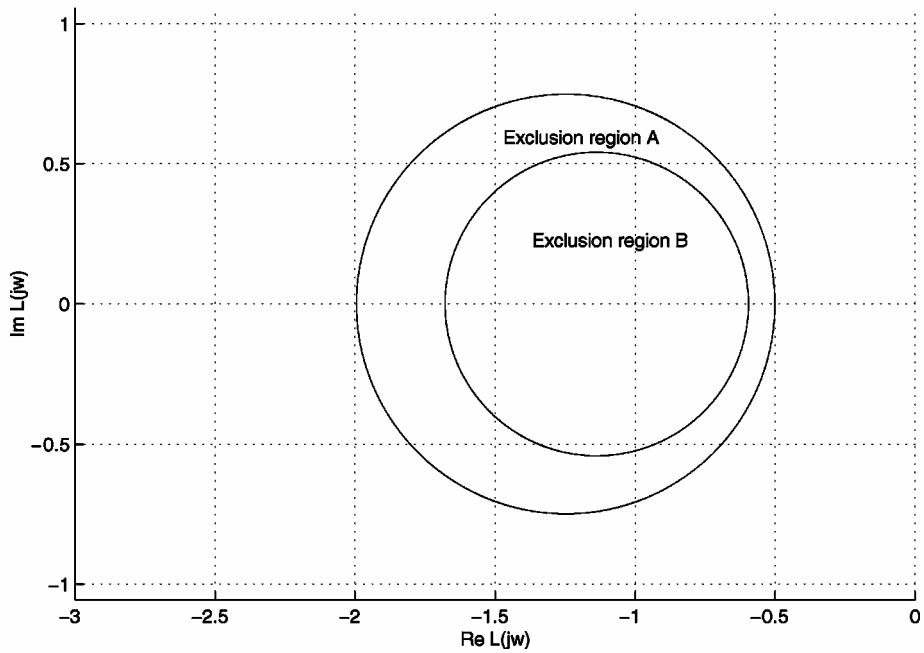

Fig. 10 Corresponding circular Nyquist plane exclusion regions.

by the open-loop frequency response $L(j\omega)$ is to consider a plant subject to disk uncertainty of (center, radius) given by $(+1.14, 0.54)$ at each frequency. It is then easy to see that avoidance of the $(-1, 0)$ critical point in the Nyquist plane by $L(j\omega)$ for all possible plants in this set is exactly equivalent to avoidance of the exclusion region B by $L(j\omega)$ for the original plant. The set of possible plants can be represented as

$$P(s) = P_1(s)(1.14 + \Delta_N) \tag{6}$$

where P_1 is the original plant, Δ_N is complex, and $\|\Delta_N\|_\infty \leq 0.54$. This is of course the same as writing

$$P(s) = 1.14P_1(s)(1 + W_N\Delta_N) \tag{7}$$

with $W_N = 0.47$ and $\|\Delta_N\|_\infty \leq 1$. In this way we can represent the Nichols exclusion region as a fictitious multiplicative input uncertainty for the scaled nominal plant. This uncertainty can then be pulled out of the closed-loop system along with all the other uncertainties to form an LFT-based representation of the uncertain system in the usual way. (See Ref. 16 for a simple example.) For single-loop analysis, the fictitious uncertainty representing the Nichols exclusion region is inserted in one loop at a time, whereas in the multiloop case it is applied to all loops simultaneously. Note that this approach allows simultaneous variations of the uncertainty in all of the loops of the system, and thus, every possible combination of the phase/gain offset is considered. In contrast, the classical approach assumes the same phase and gain margin variation in each loop and also checks for only a few points (usually the corners) in the exclusion region.

B. Trapezoidal Nichols Plane Exclusion Regions μ-Analysis

A second approach to casting Nichols plane exclusion region specifications as a μ problem was developed in Ref. 8. This method models the Nichols exclusion regions of Fig. 1 using a Padé approximation. The variations in the phase and gain are represented by Eqs. (8) and (9), respectively. The phase offset is given by

$$\phi = [(\phi_{\max} - \phi_{\min})/2]\delta_2 + [(\phi_{\max} + \phi_{\min})/2] \tag{8}$$

The gain offset a (in decibels) is represented as

$$a = \delta_1(t - m\delta_2) \tag{9}$$

where δ_1 and δ_2 are normalized real uncertainties and t and m characterize the top limit line of the exclusion region. For instance, the inner exclusion region in Fig. 1 for the single-loop analysis requires that $t = 3$ and $m = 1.5$. To cast this problem into a μ framework, it is necessary to convert these equations to the polar form $ae^{-j\phi}$, where the negative sign denotes phase lag. This gives

$$\begin{aligned} ae^{-j\phi} &= \exp[c\delta_1(t - m\delta_2) - j(\gamma_1\delta_2 + \gamma_2)] \\ &= \exp(-j\gamma_2)\exp[c\delta_1(t - m\delta_2) - j\gamma_1\delta_2] \end{aligned} \tag{10}$$

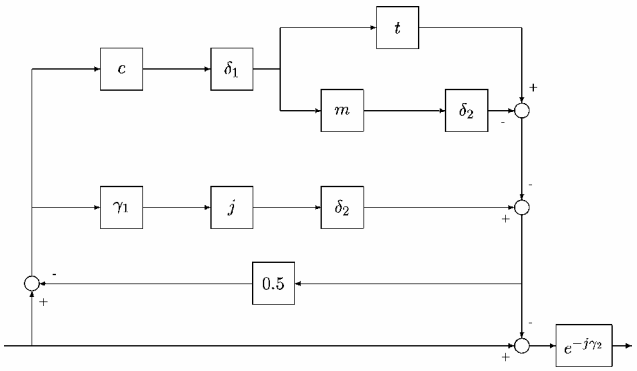

Fig. 11 LFT representation of trapezoidal Nichols exclusion region using first-order Padé approximation.

where $c = (\ln 10)/20$, $\gamma_1 = (\phi_{\max} - \phi_{\min})/2$, and $\gamma_2 = (\phi_{\max} + \phi_{\min})/2$.

To generate the LFT-based uncertainty description, a first-order Padé approximation is used:

$$\exp(-Ts) = 1 - [Ts/(1 + Ts/2)] \tag{11}$$

where $-Ts$ is given by

$$-Ts = c\delta_1(t - m\delta_2) - j\gamma_1\delta_2 \tag{12}$$

This first-order approximation is adequate for phase margins of up to 90 deg. The resulting LFT-based uncertainty model for this first-order Padé approximation is shown in Fig. 11. The uncertainty block Δ_{margins} is made up of two real scalars, δ_1 and δ_2, the latter being repeated twice,

$$\Delta_{\text{margins}} = \begin{bmatrix} \delta_1 & 0 \\ 0 & \delta_2 I_2 \end{bmatrix} \tag{13}$$

As shown in Fig. 12, this method matches the exclusion region used by the classical approach (Fig. 1) very well.

For multiloop analysis, the LFT-based uncertainty model already described is inserted in all loops simultaneously. In this case, however, the gain and phase margin requirements are 3 dB and 30 deg, respectively, and therefore, the parameters m and t from Eq. (9) are chosen as $m = 1$ and $t = 2$. The multiloop criterion is then checked by scaling the exclusion region by applying a scaling factor to m, t, γ_1, and γ_2 until $\mu = 1$. At this point, the gain and phase margins can be computed by back substituting these values in Eqs. (8) and (9).

Note that the uncertainty associated with the elliptical Nichols exclusion region is complex, and it is, therefore, necessary to use mixed-μ algorithms to compute bounds on μ in this approach. The quality of the resulting lower bounds will then depend on the amount of complex vs real uncertainty in the Δ matrix. In the case of the trapezoidal Nichols exclusion region, purely real uncertainties are introduced by the Padé approximation, and thus, this problem necessitates the use of real-μ algorithms (by the approach in Ref. 17) for generating lower bounds on μ.

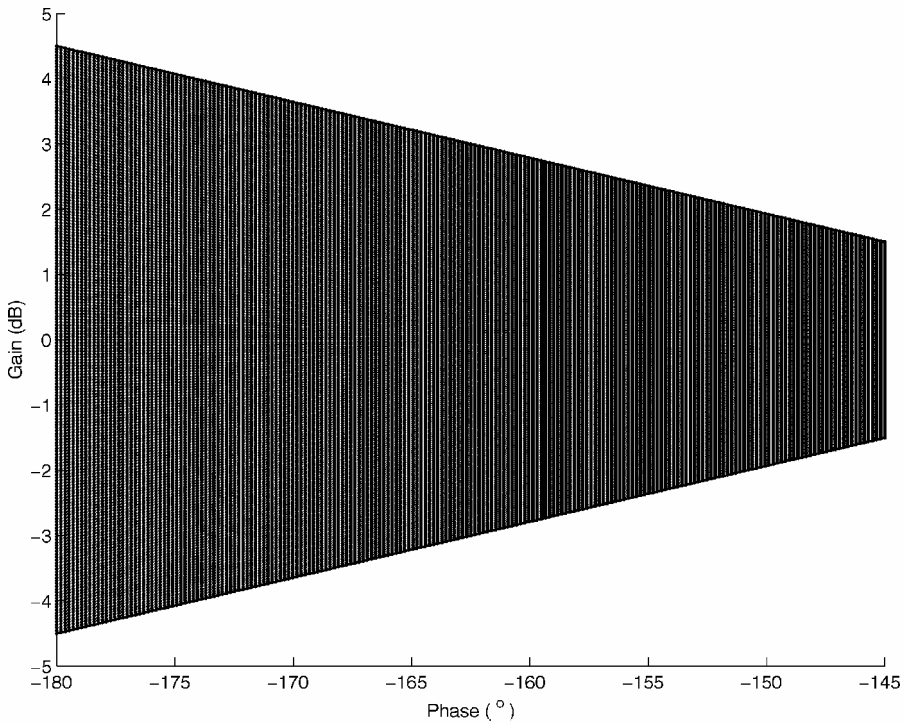

Fig. 12 Padé approximation of trapezoidal Nichols exclusion regions.

C. Worst-Case Eigenvalue Criterion μ Tools

In this section, we describe how μ-analysis methods can be used to address the worst-case eigenvalue clearance criterion defined in Sec. II. From the standard block diagram for μ analysis (Fig. 5), stability of the uncertain closed-loop system is equivalent to stability of the quantity $(I - M_{11}\Delta)^{-1}$. By testing the stability of $(I - M_{11}\Delta)^{-1}$ as the Δ_i elements vary, we can find the worst-case, or smallest, set of simultaneous changes in Δ_i that drive the system unstable. From matrix theory,

$$(I - M_{11}\Delta)^{-1} = \text{adj}(I - M_{11}\Delta)/\det(I - M_{11}\Delta)$$

Thus, for a given set of model perturbations Δ, and a given complex number s_0 that is not an open-loop pole of $M_{11}(s)$ or $\Delta(s)$, s_0 is a closed-loop pole if and only if

$$\det[I - M_{11}(s_0)\Delta(s_0)] = 0$$

Suppose we want to find the smallest set of Δ_i elements that places a pole at s_0:

$$k_m =: \min_{\Delta}\{k \in [0, \infty] \quad \text{such that} \quad \det(I - M_{11}(s_0)\Delta(s_0)) = 0\}$$

where $\Delta = \text{diag}(\Delta_1, \ldots, \Delta_p)$ and $\bar{\sigma}[\Delta_i(s_0)] \le k \; \forall \, i$

Then,

$$\mu_{\Delta}(M_{11}) = 1/k_m$$

Most published work on μ analysis has assumed that μ must be computed on a frequency sweep along the $s = j\omega$ axis. However, computing μ away from the imaginary axis can also provide a lot of useful information. In particular, the worst-case eigenvalue criterion can be checked by shifting the imaginary axis into the left- and right-half planes until an uncertainty combination is found that places a closed-loop pole on the axis. Other tests are also possible: For example, by sweeping s_0 along a line of constant damping, such as $\xi = 0.4$, one may find the smallest perturbation that reduces damping below this level. Because k_m is typically discontinuous as s_0 moves from the real axis to neighboring complex points, it is also useful to check stability along the real axis. Another useful way to present the data is to compute k_m on a grid in the s plane around a nominal closed-loop pole and then make a contour map of k_m. This shows directly how the closed-loop poles migrate in the s plane as a result of the uncertainty, that is, it corresponds to a multiparameter root locus. (See Ref. 18 for more on this approach.)

VI. Analysis of the Longitudinal HWEM Dynamics

Full results from the analysis of the longitudinal dynamics of the CL002 control law over the HWEM flight envelope can be found in Ref. 13. In this paper we focus on comparing the results obtained using the classical gridding based approaches with the results obtained using the μ-analysis tools described earlier. The analysis is carried out at the flight conditions (FC) defined in Table 1. Only the straight and level flight case is considered, taking into account the five category 1 pitch uncertainties. Because three aerodynamic uncertainties are included simultaneously, it is necessary to apply a reduction factor of 0.46 to their ranges of variation as suggested in Ref. 19.

A. Worst-Case Eigenvalue Criterion

For the considered ranges of uncertainties, this criterion was satisfied for all seven FC, and almost identical results were obtained using the μ-analysis and classical techniques. For FC1, for example, the nominal, μ worst-case and classical worst-case eigenvalue positions are shown in Table 3. Also shown in Table 3 are the worst-case

Table 3 Sample results for worst-case eigenvalue criterion at FC1

Nominal eigenvalue	Classical worst-case eigenvalues	μ worst-case eigenvalues	Classical worst-case uncertainties	μ worst-case uncertainties
-0.2	-0.1985	-0.1980	1	0.9682
-0.17	-0.1669	-0.1660	-1	-0.9985
-0.065	-0.0631	-0.0630	1	0.9771
$-0.0245 + 0.1391j$	$-8.5e{-}5 + 0.0775j$	$7.8e{-}5 + 0.0775j$	-1	-0.9906
$-0.0245 - 0.1391j$	$-8.5e{-}5 - 0.0775j$	$7.8e{-}5 - 0.0775j$	1	0.9886

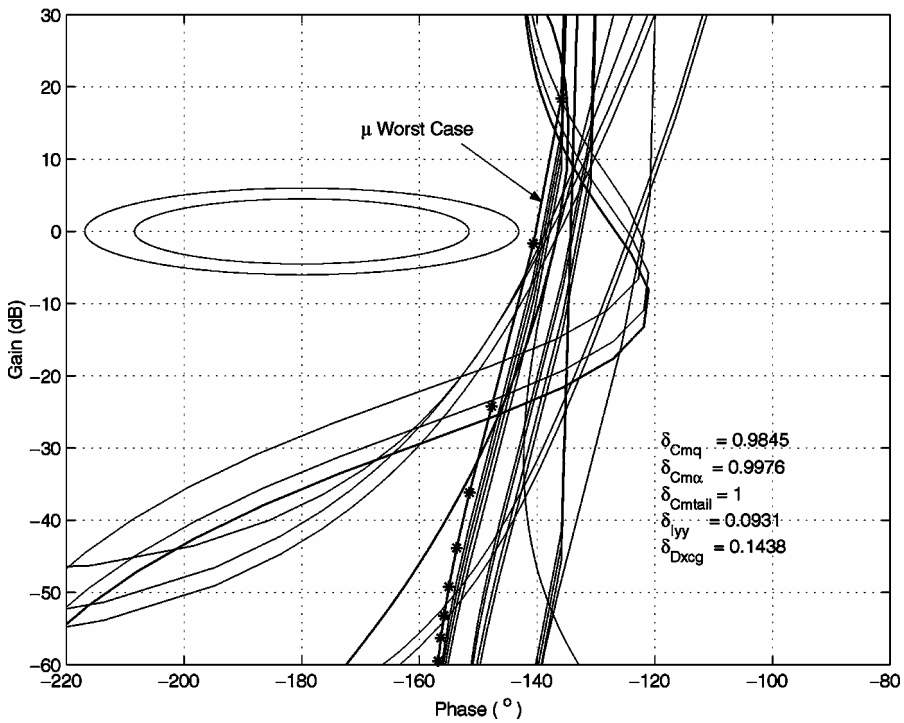

Fig. 13 Stability margin criterion for FC4: ∗, μ worst case and ——, classical.

values of the uncertain parameters found using both approaches. Note that although the results are very similar, the μ worst-case uncertainty combination places all of the eigenvalues slightly nearer the boundaries.

B. Worst-Case Stability Margin Criterion (Single-Loop Analysis)

To compare the worst-case stability margin criterion results, Nichols curves were plotted for 1) the worst case obtained using μ and 2) every combination of the extreme points of the five category 1 uncertain parameters. It was found that for three FCs (FC4, FC5, and FC6), the worst-case uncertainties did not lie on the extreme points of the parameters. The results are shown in Figs. 13–18, where the zoomed versions are shown in Figs. 14, 16, and 18, respectively. It can be seen that in all three cases, the classical approach produces optimistic results, that is, the worst-case Nichols plots found by μ are closer to the exclusion regions. For instance, the tailplane loop cut analysis at FC4 using μ (Figs. 13 and 14) generated a worst-case uncertainty of $\delta_{C_{m_q}} = 0.9845, \delta_{C_{m_\alpha}} = 0.9976, \delta_{C_{m_{\text{tail}}}} = 1, \delta_{I_{yy}} = 0.0931$, and $\delta_{X_{Dx\,\text{cg}}} = 0.1438$. When the classical approach was used, the worst case was found to be $\delta_{C_{m_q}} = 1, \delta_{C_{m_\alpha}} = 1, \delta_{C_{m_{\text{tail}}}} = 1, \delta_{I_{yy}} = -1$,

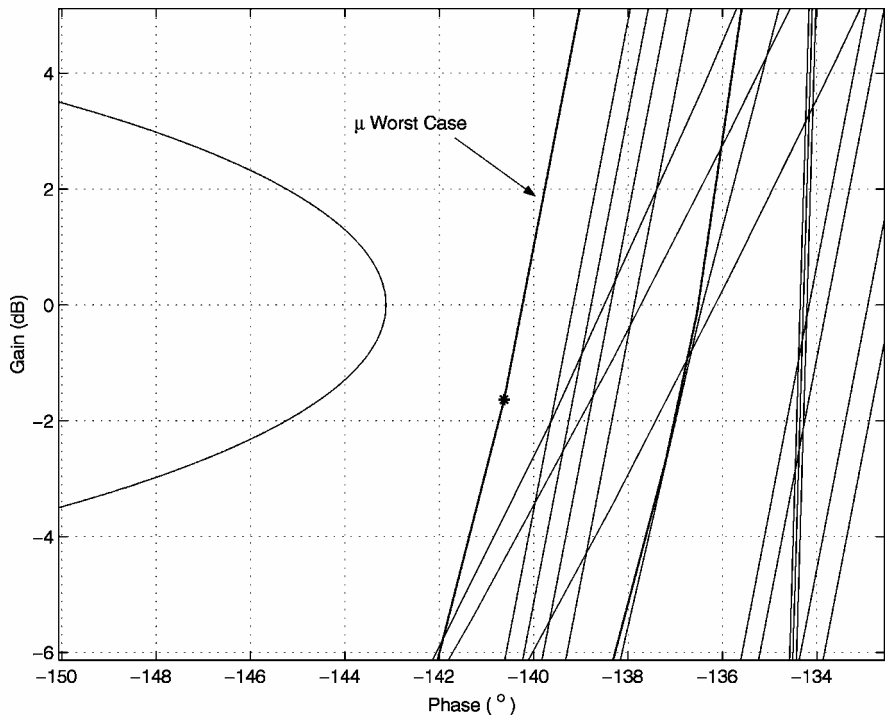

Fig. 14 Closeup of Fig. 13.

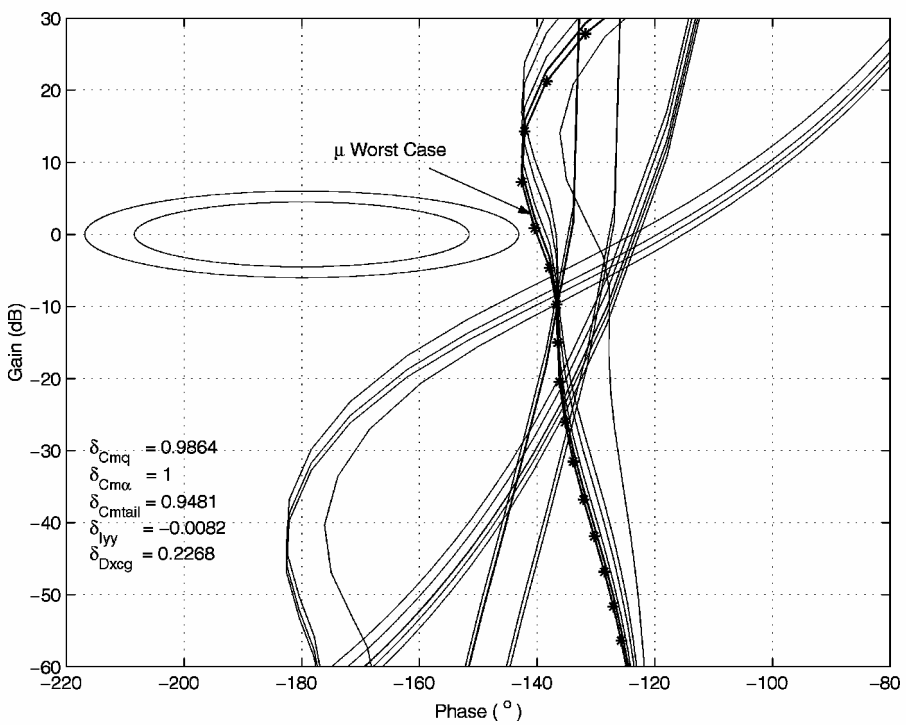

Fig. 15 Stability margin criterion for FC5: ∗, μ worst case and ——, classical.

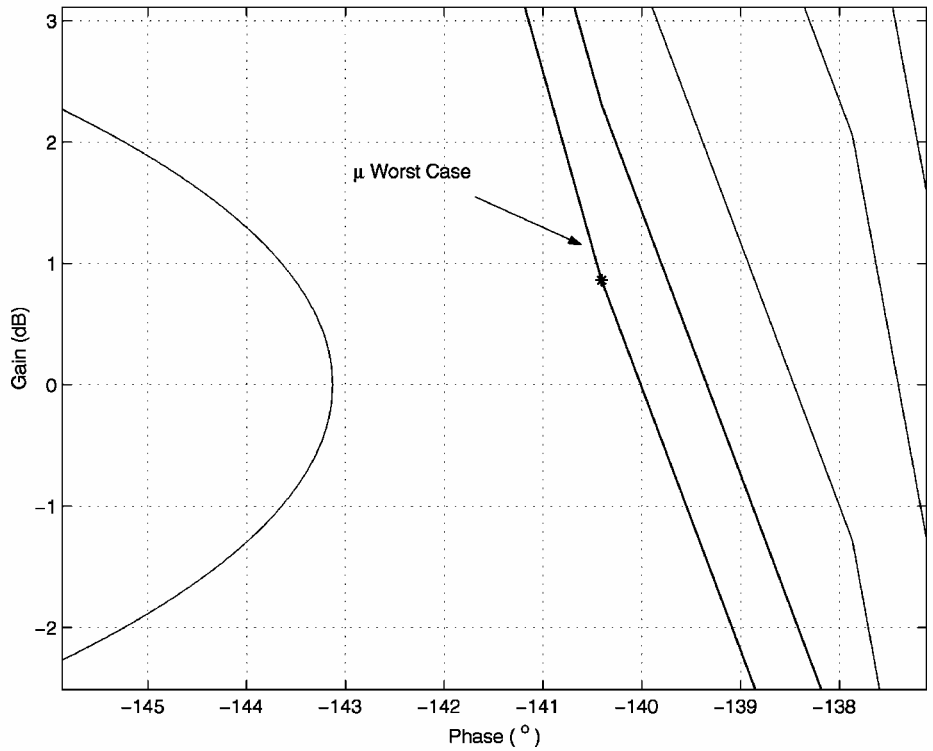

Fig. 16 Closeup of Fig. 15.

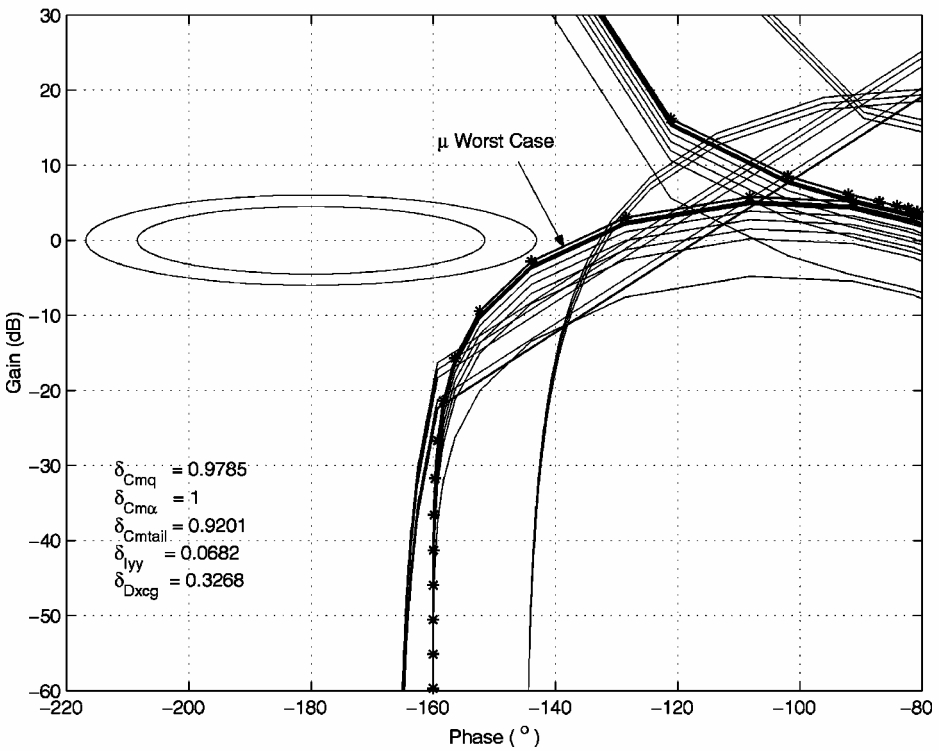

Fig. 17 Stability margin criterion for FC6: ∗, μ worst case and ——, classical.

and $\delta_{X_{cg}} = 1$. The question then arises as to how important the last two uncertainties are, that is, whether $\delta_{I_{yy}}$ and $\delta_{X_{cg}}$ have a significant effect on the stability margins. This question can be easily answered using the technique of μ sensitivities,[20] which measures the relative importance of each uncertainty in the Δ set. Table 4 shows that $\delta_{X_{cg}}$ and $\delta_{I_{yy}}$ are rated the second and third most important elements in the set, implying that changes in the values of these two parameters will significantly affect the stability margins. Note again that the

Table 4 μ sensitivities

Uncertainty	μ sensitivities
$\delta_{C_{m_\alpha}}$	0.2328
$\delta_{X_{cg}}$	0.1797
$\delta_{I_{yy}}$	0.0287
$\delta_{C_{m_q}}$	0.0251
$\delta_{C_{m_{tail}}}$	0.0001

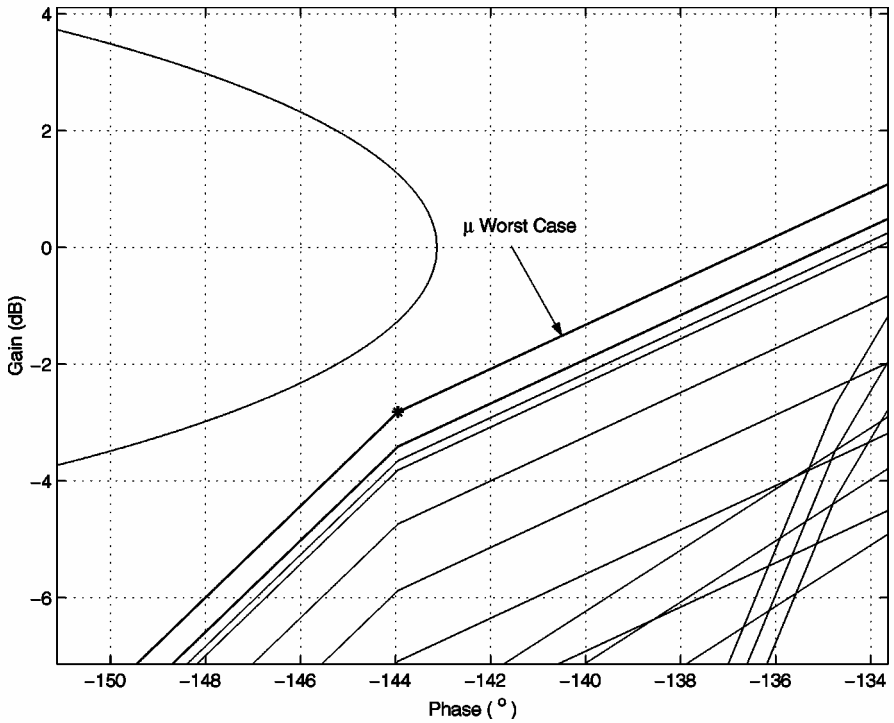

Fig. 18 Closeup of Fig. 17.

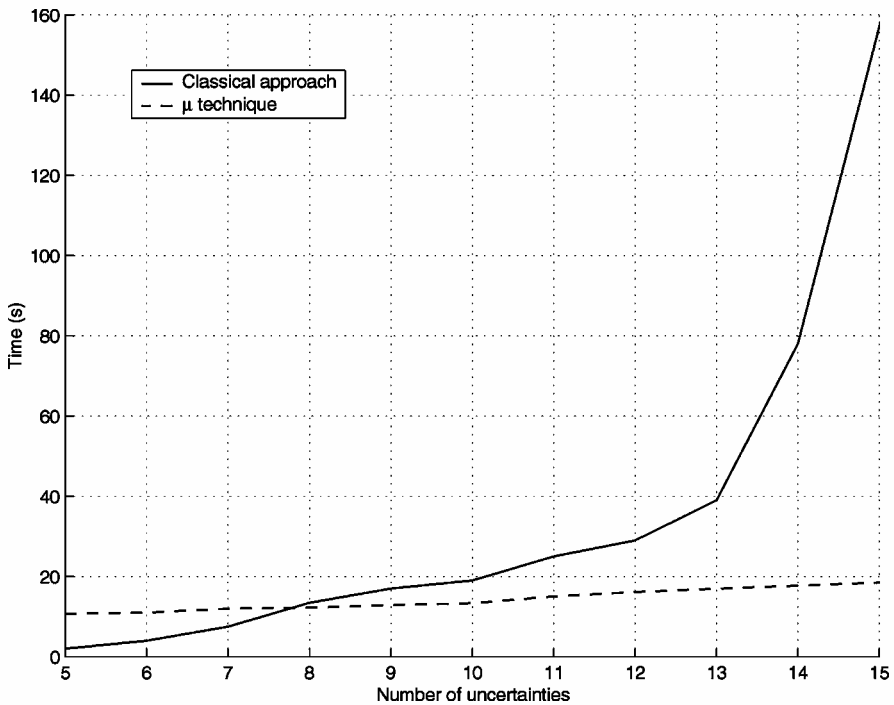

Fig. 19 Computation times for μ and classical techniques.

values of these parameters that give the true worst case do not correspond to thir maximum or minimum values. This phenomonon is repeated for all three of the FCs shown in Figs. 13–17 and calls into question the implicit assumption made in the classical approach that the worst case will always correspond to some combination of the extrema of the uncertain parameters.

The computation times for finding the worst cases was recorded for 1) the classical approach using only minimum and maximum values of each parameter and 2) μ analysis with 100 frequency points. The results are plotted in Fig. 19. As expected, the computation time for the classical approach increases exponentially with the number of uncertainties, so that for a Δ size > 8, μ is seen to be less computationally intensive than the classical technique. This fact becomes significant when we seek to also include category 2 uncertainties in the analysis, or when we seek to analyze the effect of longitudinal and lateral uncertainties together. Figure 20, for example, shows the analysis results for the 10 combined longitudinal and lateral category 1 uncertainties. In this case, the same worst-case is found by both approaches. The μ-analysis method, however, is almost 30% faster.

C. Worst-Case Stability Margin Criterion (Multiloop Analysis)

In the following, we present sample results for the worst-case stability margin multiloop analysis, at FC5, using the elliptical Nichols

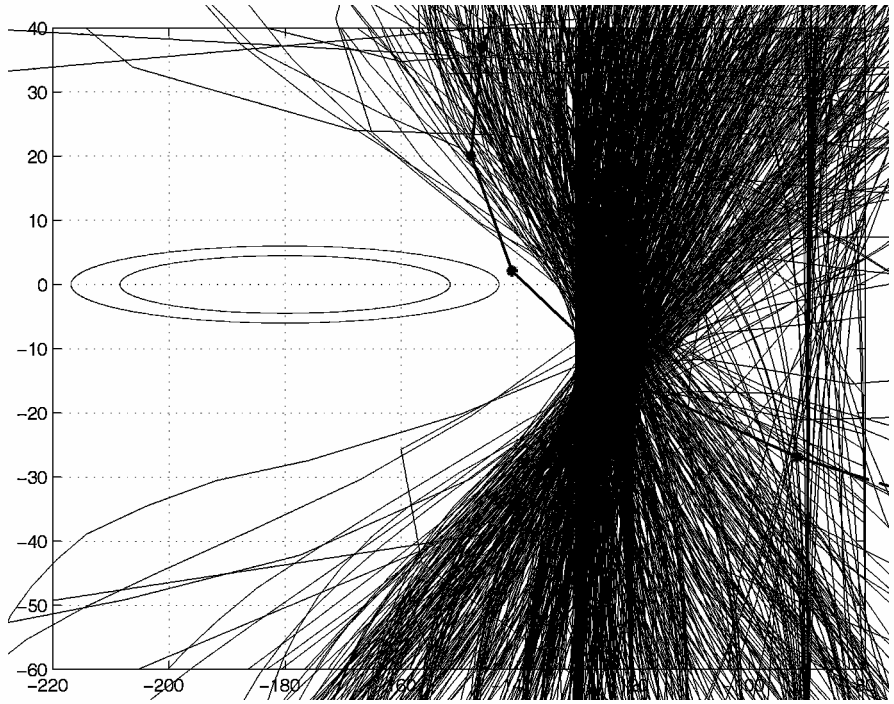

Fig. 20 Stability margin criterion for 10 uncertain parameters: $*$, μ worst case and ——, classical.

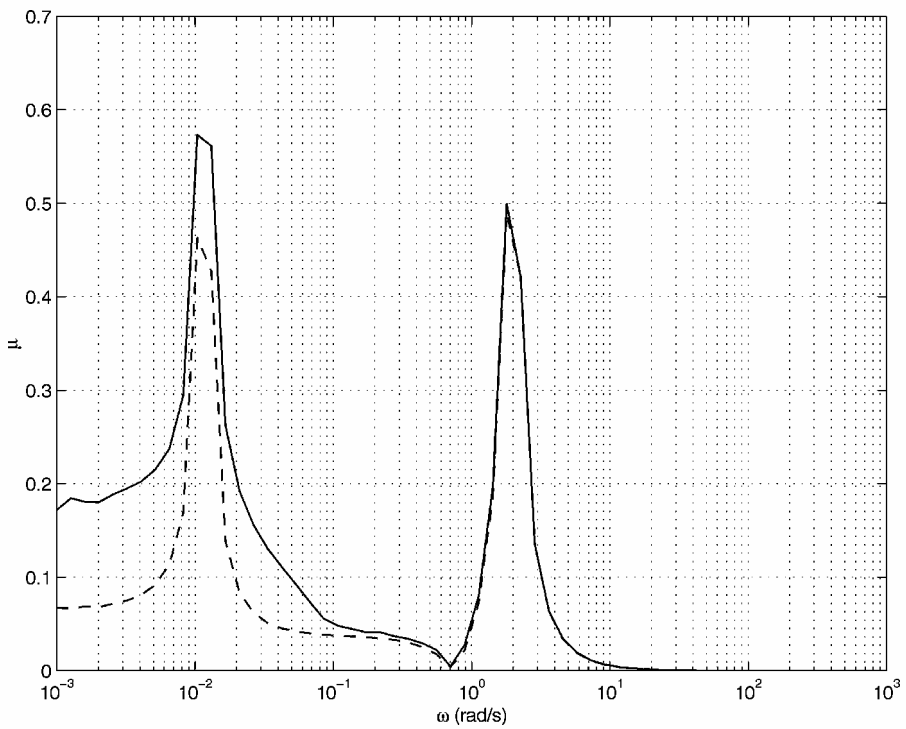

Fig. 21 Mixed μ bounds for the elliptical Nichols exclusion region test.

plane exclusion regions. When the μ-analysis approach was used, the uncertainties associated with the elliptical Nichols exclusion regions were increased in each loop simultaneously until $\mu = 1$. The corresponding gain and phase margins were found to be 13.97 dB and 37.86 deg, respectively. When the classical approach was used, the corner points of the trapezoidal Nichols exclusion region were checked, and the gain and phase margins were computed as 15.5 dB and 41.2 deg, respectively. Observe that the results obtained using the classical approach are more optimistic than those computed from μ. The explanation for these differences is twofold. First, every possible combination of the phase/gain offsets is considered in the μ analysis, whereas the classical approach assumes the same phase/gain variations in each loop of the system. Second, the μ analysis imposes a slightly more stringent requirement on the computation of the phase and gain margins (because the elliptical exclusion regions used by μ are slightly bigger than the diamond-shaped exclusion regions used by the classical approach).

D. Elliptical vs Trapezoidal Nichols Exclusion Regions

To get a clearer picture of the effect of using different shaped exclusion regions, a comparison of μ-analysis results for both regions was made, for both single-loop and multiloop cases. For a tailplane loop cut at FC2, the resulting mixed-μ bounds are shown in Fig. 21 for the elliptical exclusion region test, whereas the real-μ bounds are shown in Fig. 22 for the trapezoidal exclusion

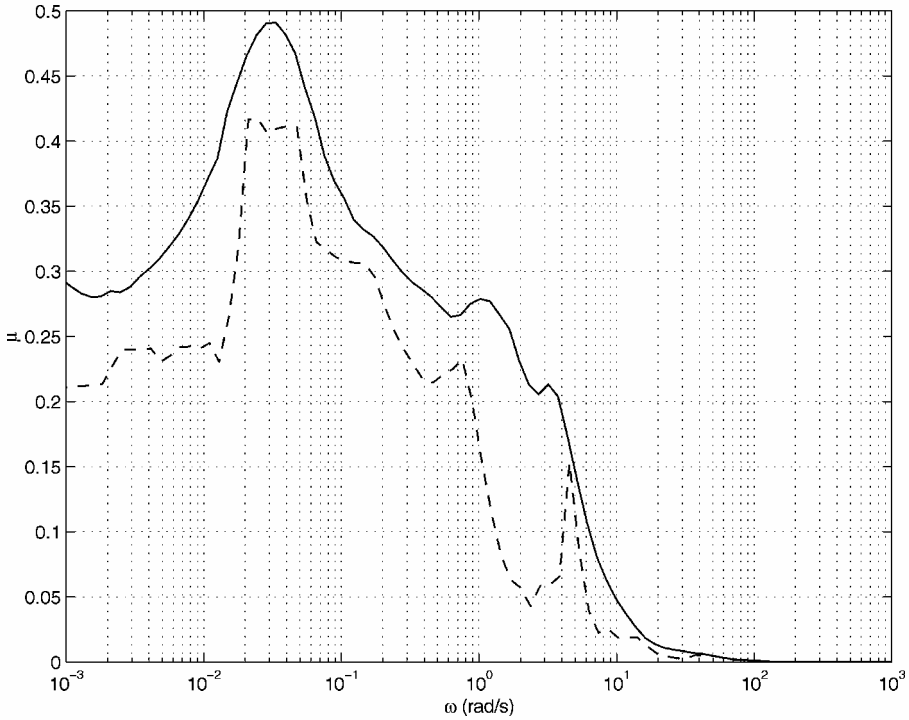

Fig. 22 Real μ bounds for the trapezoidal Nichols exclusion region test.

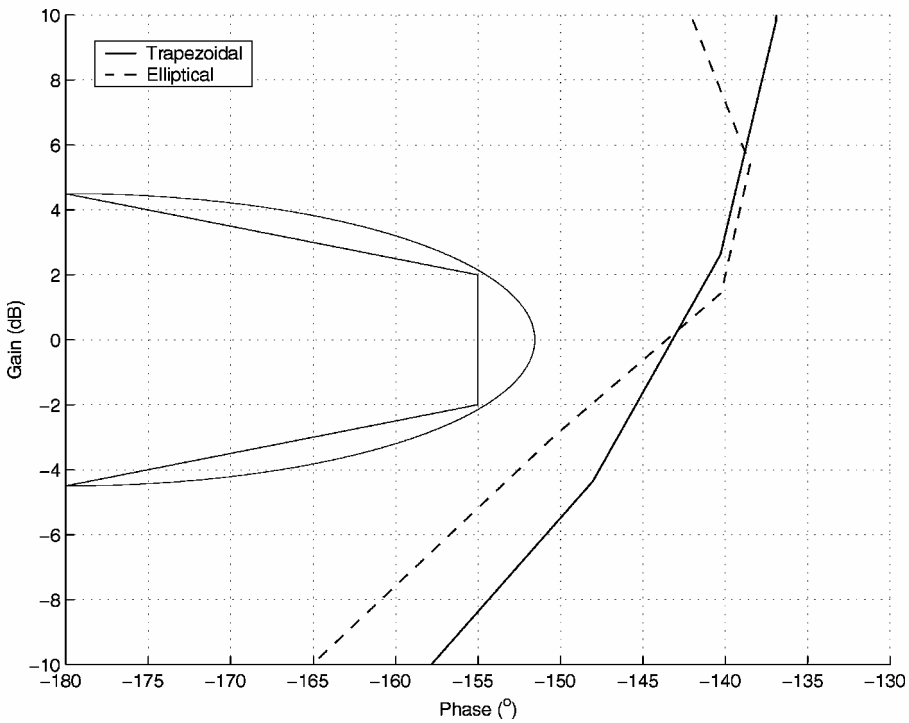

Fig. 23 Worst-case Nichols plots for tailplane loop cut for different exclusion regions.

region test. The different exclusion regions as well as the corresponding worst-case Nichols plots are shown in Fig. 23. Interestingly, quite different worst cases were obtained for the two regions: The worst-case parameter combination for the elliptical exclusion region test was found to be $\delta_{C_{m_q}} = 2.0504$, $\delta_{C_{m_\alpha}} = 1.4291$, $\delta_{C_{m_{\text{tail}}}} = 2.0369$, $\delta_{I_{yy}} = 1.0262$, and $\delta_{X_{D\text{xcg}}} = 0.3548$, whereas that of the trapezoidal exclusion region test was identified as $\delta_{C_{m_q}} = 2.2716$, $\delta_{C_{m_\alpha}} = 1.9934$, $\delta_{C_{m_{\text{tail}}}} = 2.2119$, $\delta_{I_{yy}} = 1.8133$, and $\delta_{X_{D\text{xcg}}} = 0.6113$.

A multiloop μ analysis was also carried out using the elliptical and trapezoidal Nichols exclusion regions. Both exclusion regions were scaled until the value of μ reached 1, and the resulting phase and gain margins were then computed. For the elliptical Nichols exclusion region test, a phase margin of 41.2 deg and a gain margin of 4.18 dB were obtained. For the trapezoidal Nichols exclusion region test, a phase margin of 44.8 deg and a gain margin of 4.5 dB were obtained. Again, it can be observed that the elliptical exclusion region is, as expected, slightly more conservative than the trapezoidal exclusion region.

VII. Conclusions

This paper has described new μ-analysis tools for the clearance of flight control laws for highly augmented aircraft. These tools have been used to analyze the stability robustness properties of a flight control law for a vertical/short takeoff and landing aircraft.

Comparisons between the μ-analysis techniques and the classical industrial approach show that the new analysis tools can provide more rigorous, that is, more accurate identification of worst cases, and efficient, that is, computationally faster, analysis of worst-case aircraft stability characteristics in the presence of multiple sources of parametric uncertainty. A particularly interesting aspect of the results described in the paper is that worst cases were shown by the μ tools to sometimes occur in the interior of the uncertain parameter space, that is, not at some combination of the extreme values of the uncertain parameters. This result contradicts the basic assumption of the classical gridding approach, and further motivates the use of the proposed new analysis tools.

Acknowledgment

The authors are grateful to Glenn D'Mello from Qinetiq, Ltd., for many helpful discussions on the vectored-thrust aircraft advanced flight control Harrier model and control law CL002.

References

[1]Korte, U., "Tasks and Needs of the Industrial Clearance Process," *Advanced Techniques for Clearance of Flight Control Laws*, edited by C. Fielding, A. Varga, S. Bennani, and S. Selier, Lecture Notes in Control and Information Sciences, No. 283, Springer-Verlag, Berlin, 2002, Chap. 2, pp. 13–33.

[2]Hyde, R. A., *H^∞ Aerospace Control Design—A VSTOL Flight Application*, Springer-Verlag, Berlin, 1995, pp. 123–202.

[3]Papageorgiou, G., Glover, K., D'Mello, G., and Patel, Y., "Taking Robust LPV Control into Flight on the VAAC Harrier," *IEEE Conference on Decision and Control*, IEEE Publ., Piscataway, NJ, 2000.

[4]D'Mello, G., "The Harrier Wide Envelope Model," GARTEUR TP-119-08, URL: http://www.nlr.nl/public/hosted-sites/garteur/rfc.html [2002].

[5]D'Mello, G., "Selected Criteria For Clearance of the HWEM Flight Control Laws," GARTEUR TP-119-08-A, URL: http://www.nlr.nl/public/hosted-sites/garteur/rfc.html [2002].

[6]Ferreres, G., *A Practical Approach To Robustness Analysis*, Kluwer Academic/Plenum, Boston, 1999, pp. 43–52.

[7]Varga, A., Looye, G., Moormann, D., and Grübel, G., "Automated Generation of LFT-based Parametric Uncertainty Descriptions from Generic Aircraft Models," GARTEUR TP-088-36, http://www.nlr.nl/public/hosted-sites/garteur/rfc.html [1997].

[8]Mannchen, T., Petermann, C., Weinert, B., and Zobelein, T., "Flight Control Law Clearance of the HIRM + Fighter Aircraft Model using μ-Analysis," GARTEUR TP-119-12, URL: http://www.nlr.nl/public/hosted-sites/garteur/rfc.html [2001].

[9]Mannchen, T., Bates, D. G., and Postlethwaite, I., "Modeling and Computing Worst-Case Uncertainty Combinations for Flight Control Systems Analysis," *Journal of Guidance, Control, and Dynamics*, Vol. 26, No. 6, 2002, pp. 1029–1039.

[10]Dijkgraaf, J. P., "Generation of Low Order HIRMplus LFT Models: An Application of the LFR Toolbox," GARTEUR TP-119-20, URL: http://www.nlr.nl/public/hosted-sites/garteur/rfc.html [2001].

[11]Kureemun, R., Bates, D. G., and Hayes, M. J., "On the Generation of LFT-Based Uncertainty Models for Flight Control Law Robustness Analysis," AIAA Paper 2001-4396, 2001.

[12]Morton, B., "New Applications of μ to Real-Parameter Variation Problems," *24th IEEE Conference on Decision and Control*, IEEE Publ., Piscataway, NJ, 1985, pp. 233–238.

[13]Kureemun, R., "μ-Analysis Tools for the Flight Clearance of Highly Augmented Aircraft," Ph.D. Dissertation, Dept. of Engineering, Univ. of Leicester, Leicester, England, U.K., Nov. 2002.

[14]Deodhare, G., and Patel, V. V., "A 'Modern' Look at Gain and Phase Margins: an $\mathcal{H}^\infty/\mu$ Approach," AIAA Paper 98-4134, 1998.

[15]Kureemun, R., Bates, D. G., and Postlethwaite, I., "Quantifying the Robustness of Flight Control Systems Using Nichols Exclusion Regions and the Structured Singular Value," *IMechE Journal of Systems and Control Engineering*, Vol. 215, No. 16, 2001, pp. 625–638.

[16]Bates, D. G., and Postlethwaite, I., *Robust Multivariable Control of Aerospace Systems*, Delft Univ. Press, Delft, The Netherlands, 2002, pp. 78–88.

[17]Hayes, M. J., Bates, D. G., and Postlethwaite, I., "New Tools for Computing Tight Bounds on the Real Structured Singular Value," *Journal of Guidance, Control, and Dynamics*, Vol. 24, No. 6, 2001, pp. 1204–1213.

[18]Dailey, R., and Gangsaas, D., "Worst Case Analysis of Flight Control Systems Using the Structured Singular Value," AIAA Paper 89-49406, 1989.

[19]Karlsson, F., Korte, U., and Scala, S., "Selected Criteria for Clearance of the HIRMplus Flight Control Laws," GARTEUR TP-119-2A1, URL: http://www.nlr.nl/public/hosted-sites/garteur/rfc.html [2001].

[20]Braatz, R. D., and Morari, M., "μ-Sensitivities as an Aid for Robust Identification," *Proceedings of the American Control Conference*, Vol. 1, IEEE Publ., Piscataway, NJ, 1991, pp. 231–236.